



# The mechanism for the serrated flow induced by Suzuki segregation in a Ni alloy

Zhouwen Jiang<sup>a</sup>, Lilong Zhu<sup>b,c</sup>, Lianxu Yu<sup>d</sup>, Baoan Sun<sup>e</sup>, Yang Cao<sup>f</sup>, Yonghao Zhao<sup>f,\*\*</sup>,  
Yong Zhang<sup>a,\*</sup>

<sup>a</sup> Herbert Gleiter Institute of Nanoscience, School of Materials Science and Engineering, Nanjing University of Science and Technology, Nanjing, 210094, China

<sup>b</sup> Institute for Advanced Studies in Precision Materials, Yantai University, Yantai, 264005, China

<sup>c</sup> State Key Laboratory of Powder Metallurgy, Central South University, Changsha, 410083, China

<sup>d</sup> Metalink International Co, Ltd, Nanjing, 211153, China

<sup>e</sup> Institute of Physics, Chinese Academy of Sciences, Beijing, 100190, China

<sup>f</sup> Nano and Heterogeneous Materials Center, School of Materials Science and Engineering, Nanjing University of Science and Technology, Nanjing, 210094, China

## ARTICLE INFO

### Keywords:

Ni alloy  
Stacking fault  
Dynamic strain ageing  
Segregation  
Mechanical properties

## ABSTRACT

The occurrence of serrated flow has been well accepted as a prevailing deformation feature in Ni-based alloys during plastic deformation at intermediate temperatures, yet its microstructure origin remains poorly understood. Here, characteristics of dynamic strain aging (DSA) in a Ni alloy 230 are studied by tensile tests over a wide range of temperatures and strain rates. The activation energy,  $Q$ , of the DSA effect is calculated to be 104 kJ/mol for temperatures from 523 to 773 K, about 35%–50% of the activation energy for lattice diffusion of Cr, Co or Mo in Ni, indicating pipe diffusion to be the crucial mode for solute segregation. Enrichment of Cr and Co atoms at stacking faults investigated by the state-of-the-art energy dispersive X-ray (EDX) spectroscopy is found in the deformed samples at 773 K with the strain rate of  $3 \times 10^{-3} \text{ s}^{-1}$ , suggesting that dynamic interactions between dissociated dislocations and substitutional solute atoms, known as Suzuki segregation, is responsible for the DSA effect. Moreover, the calculated diffusion distances of solute atoms through bulk diffusion prove that the pipe diffusion along partial dislocation core is contributing to the tensile process.

## 1. Introduction

Nickel-based Alloy 230 is a solid-solution strengthened superalloy originally developed in the 1980's for applications in aerospace, power plant and chemical processing industries (e.g. Intermediate Heat Exchanger) because of its superior high-temperature strength, corrosion resistance and oxidation resistance [1]. It was reported earlier that repetitive "serrations" on the flow stress curves are one of the predominant characteristics for the deformation of alloy 230 at intermediate temperatures with a wide range of strain-rates [1]. The serrations are categorized in terms of the well-recognized nomenclature in literatures [2–9]. Type A serrations are periodic serrations arising from the repetitive deformation bands initiating and propagating from one end to the other end of the gage section. These are locking serrations characterized by a steep rise in stress followed by a drop to or below the general level of the stress-strain curve. Type B serrations are also considered as

locking serrations, but characterized with successive oscillations about the general level of the stress-strain curve due to the hopping propagation of the localized deformation bands in the gage length. Type C serrations are yield drops that occur below the general level of the flow curve, and therefore considered as unlocking serrations [2–9]. The occurrence of serrated flow has been well accepted as a prevailing deformation feature in Ni-based alloys during plastic deformation at intermediate temperatures [3–7,10–18]. The repeated serrations appearing on the stress strain curves are a manifestation of localized plastic deformation in the tensile specimen gauge section, which may influence the mechanical properties, such as strength, ductility and surface quality [2–7,11–19].

Numerous investigations have been performed to understand the mechanism responsible for the serrated phenomenon in Ni alloys [3–7, 10–17,20]. The consensus exist is that the serrated flow during tensile deformation, usually referred to as the Portevin-Le Chatelier (PLC)

\* Corresponding author.

\*\* Corresponding author.

E-mail addresses: [yhzhaonjust.edu.cn](mailto:yhzhaonjust.edu.cn) (Y. Zhao), [yong@njust.edu.cn](mailto:yong@njust.edu.cn) (Y. Zhang).

effect, can be ascribed to the dynamic strain aging (DSA), arising from interactions between mobile dislocations and diffusing solute atoms during plastic flow in Ni alloys [3–7,11–16,21–23] and Al alloys [9, 24–26]. The critical strain for the onset of serrated flow,  $\varepsilon_c$ , depending on the deformation temperatures and strain rates. At low temperatures and at high strain rates,  $\varepsilon_c$  increases with increasing  $\dot{\varepsilon}$  and decreasing  $T$ , which is referred to as the normal PLC effect. On the other hand, at high temperatures and low strain rates,  $\varepsilon_c$  increases with increasing  $T$  and decreasing  $\dot{\varepsilon}$  (inverse PLC effect) [4–6,10,13,15,16,19,24]. The activation energy,  $Q$ , for serrated flow, which can be determined by using  $\varepsilon_c$  for the onset of serrations (or average stress drop ( $\Delta\sigma_{avg}$ ) associated with serrations), has essentially been utilized to deduce the solute atmosphere species responsible for the DSA [3,4,6,8,11–13,21,22]. Following these methods, Hayes et al. [21] attributed the DSA in solution-annealed Inconel 600 and aged Inconel 718 to the diffusion of interstitial C atoms at temperatures lower than 866 K, and of Cr and Nb atoms at higher temperatures, respectively. Hale et al. [13] identified the lattice diffusion of C atoms below 750 K, and of substitutional Cr atoms at higher temperatures, as being responsible for the serrated behaviors in annealed alloy 718. Nonetheless, a quick survey on existing literature suggests that there exist uncertainties of inferring the solute atoms responsible for serrated flow from the calculated activation energies, especially for the deduction of solute atoms for DSA at the low temperature regime [3,4,6,11–13]. For example, Gopinath and co-workers [11] investigated the characteristics of DSA effects in an alloy 720Li containing Cr, Co, Ti, Mo, C elements, and determined the activation energy for serrated flow below 723 K to be  $\sim 80$  kJ/mol. Although the average activation energy obtained for alloy 720Li is close to that (69 kJ/mol) for pipe diffusion of C in Ni [27], which suggests that C atoms might be responsible for the DSA effects in alloy 720Li. Nevertheless, DSA effects due to fast diffusion of C atoms begin to occur at low  $T$  of about 373 K in carbon steels [28,29]. Therefore, it is reasonable to expect that the locking behaviors induced by interstitial C atoms would lead to the occurrence of serrated flow at lower temperatures than experimental observation of  $T > 523$  K for alloy 720Li, where dislocation locking may be attributable to substitutional elements. Similar conclusions were also made in other Ni alloys [3,4,6], such as alloy 625, Nimonic 263, UNS N10276. Obviously, although it is widely accepted that the serrated flow is induced by dynamic interactions between mobile dislocations and diffusing solute atoms during plastic flow, the uncertainties concerning the solute species responsible for the DSA still persists due to the lack of direct experimental evidence.

Alloy 230, containing several substitutional elements (Cr, Co, Mo, W) and interstitial element (C), offers an opportunity to investigate the characteristics of DSA and probe the solute atmosphere species interacting with mobile dislocations. First of all, in the present work the activation energy for the onset of serrated flow in the normal PLC effect regime is determined by the plots of  $\varepsilon_c$  vs. strain rates as well as temperatures. And the solute atoms which might be responsible for the DSA phenomenon would be deduced based on the comparison of the measured activation energy with that for the lattice diffusion of solute atoms in Ni matrix. Following this, a state-of-the-art energy dispersive X-ray (EDX) spectroscopy combined with high angle annular dark field (HAADF) imaging was conducted to examine the chemical fluctuation behavior across defects in the sample tensile-deformed at 773 K with a strain rate of  $3 \times 10^{-3} \text{ s}^{-1}$ . The transmission electron microscopy (TEM) analysis will be used to clarify the deduced solute atoms based on the measured activation energy and the segregation mechanism of solute atoms for the DSA effect at 773 K.

## 2. Experimental

### 2.1. Materials

The material used in this study is a polycrystalline Ni alloy 230 with a nominal composition (in wt.%): 22.8 Cr, 13.4 W, 2.08 Mo, 1.15 Co, 0.46

Mn, 0.26 Al, 0.23 Fe, 0.27 Si, 0.09C, 0.05 Ti, 0.011 P, 0.005 S and Ni as balance. The alloy was subjected to a solution treatment at 1495 K for 1 h followed by water quenching, and the resultant microstructure is characterized by an average grain size of  $\sim 51 \mu\text{m}$ . Dog-bone tensile specimens with a gage section of  $\phi 4 \text{ mm} \times 20 \text{ mm}$  were machined from the cylindrical blanks which have been solution-treated. Tensile tests were performed on an Instron 100 kN tensile machine with strain rates of  $1 \times 10^{-2}$ ,  $3 \times 10^{-3}$ ,  $3 \times 10^{-4}$  and  $3 \times 10^{-5} \text{ s}^{-1}$  at temperatures ranging from 300 to 973 K.

Sample slices for TEM characterization were taken parallel to the tensile axis at the gage section of the deformed materials. Then, the sample slices were mechanically polished with SiC papers, and were subsequently electropolished to have electron transparent areas for purpose of TEM analysis. Electropolishing was performed in a Struers Tenupol-5 twin-jet polishing unit, using an electrolyte containing 85% ethanol and 15% perchloric acid, at a temperature of  $-20 \text{ }^\circ\text{C}$  and a voltage of 20 V. Conventional TEM observations were performed on a FEI Tecnai 20 microscope operated at 200 kV. HAADF imaging and atomic-resolution EDX spectroscopy were carried out in a FEI Titan G2 60–300 equipped with a Super-X EDX system having four Bruker silicon drift detectors.

## 3. Results

### 3.1. Serrated flow

Fig. 1 displays the typical true stress-strain curves at strain rates of  $3 \times 10^{-3} \text{ s}^{-1}$  and  $3 \times 10^{-4} \text{ s}^{-1}$ , respectively. In spite of the strain rate employed, the flow curves remained smooth at room temperature. Serrations appeared on the flow curves in the temperature range of 573–973 K. At the strain rate of  $3 \times 10^{-4} \text{ s}^{-1}$ , type A serrations prevail at 573 K (see Fig. 1b and d). Types of serrations switch to type (A + B) at 673 K and type B at 773 K, respectively. Type C serrations become prominent progressively with increasing temperatures to 873 K and above. It has been recognized that the “ageing” of the dislocations would take place during the waiting time of the dislocations at discrete obstacles rather than during their actual motion [30,31]. When the diffusion coefficient of the solute atoms is high enough to saturate the dislocation with a solute atmosphere during the waiting time at obstacles, serrated flow will start [2]. Based on the models proposed by Sleswyk [30], McCormick [31] and Jiang [9], the serration types change from type A to C with increasing temperatures due to the enhanced diffusion coefficients of solute atoms at elevated temperatures. At low temperatures, the “ageing” of dislocations occurs at relatively high critical strain only when the sufficient dislocation obstacles allow enough waiting time of dislocations for the low diffusion rate of solutes. The low diffusion coefficient also results in unsaturated solutes atmosphere, indicating type A pinning serrations characterized by a slight rise in stress followed by a drop to or below the general level of the stress-strain curve. At higher temperatures, the mobile dislocations may already carry unsaturated solutes because of the higher diffusion rate of solutes, and more solutes gather at the dislocations once meeting the obstacles, emerging type B serrations characterized with successive oscillations about the general level of the stress-strain curve. When the temperature is high enough for the mobile dislocations to absorb solutes from the start of the deformation and the saturated atmosphere formed. In this situation, type C serrations occur as yield drops below the general level of the flow curve, and therefore considered as unpinning serrations. However, at 923 K with the strain rate of  $3 \times 10^{-4} \text{ s}^{-1}$ , type C serrations occur in the following sequences of setting in at the initial stage of deformation, diminishing with straining to several percent of elongation. Fu et al. [24] proposed two critical mechanisms of PLC effect in an Al–Mg alloy in the temperature domains based on the shape of serrations on stress-strain curves. If the strength of the solute obstacles due to DSA is described by  $\sigma_{sol}$ , and the part of applied stress which contributes to unpinning is denoted as  $\sigma_{unp}$ , then the unpinning happens

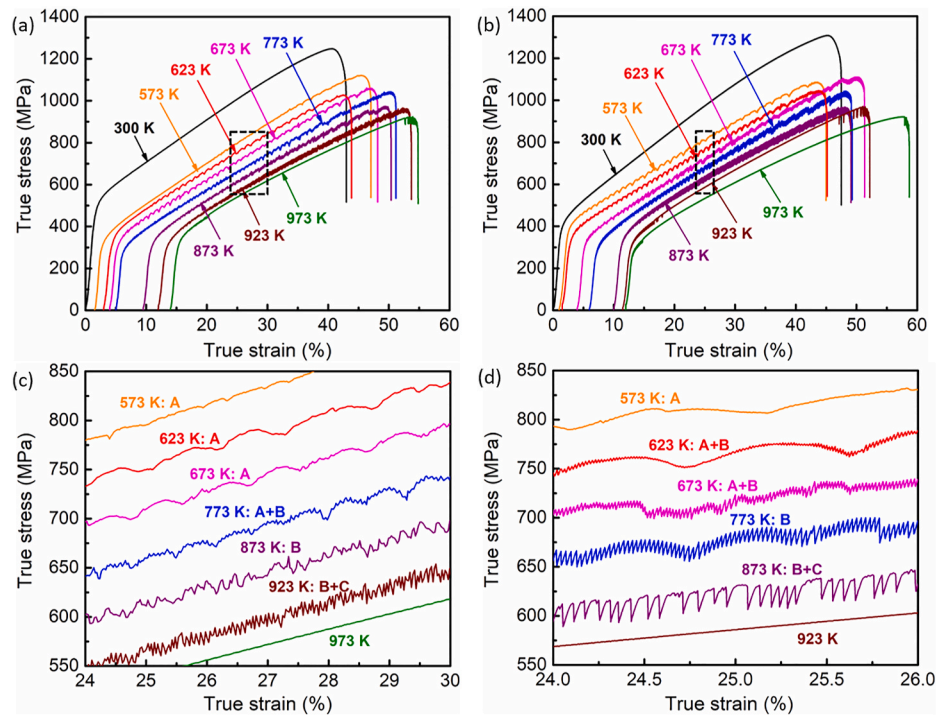


**Fig. 1.** True stress-strain curves within various temperatures and strain rates. Typical true stress-strain curves obtained at various temperatures with strain rates of (a)  $3 \times 10^{-3} \text{ s}^{-1}$  and (b)  $3 \times 10^{-4} \text{ s}^{-1}$ , and (c), (d) partial magnified views of the stress-strain curves obtained from (a), (b).

when  $\sigma_{unp}$  reaches the strength of the solute obstacles,  $\sigma_{sol}$ . Therefore, the suppression of the serrations on the early stage of the curve at 923 K may be attributed to the excessive strength of the solute obstacles with increasing temperatures and the unpinning cannot happen as a result of  $\sigma_{unp} < \sigma_{sol}$ . Similar serrated behaviors were observed on the stress-strain curves at the higher strain rate, i.e.,  $3 \times 10^{-3} \text{ s}^{-1}$ , nonetheless, lowering strain rate of  $3 \times 10^{-4} \text{ s}^{-1}$  promotes the occurrence and transition of various types of serrations at lower temperatures and increases  $\Delta\sigma_{avg}$  (see Fig. 1b and d). The detailed observations made on the serrations apparent on the flow curves are summarized in Table 1, and it agrees well with the general trend of other Ni alloys in literatures [3,13].

Serrated flow is generally seen to occur once a critical strain,  $\epsilon_c$ , for the onset of the serration is reached, which corresponds to the peak of the first serration arisen (when  $\Delta\sigma$  is greater than 1 MPa).  $\epsilon_c$  depends on both temperatures and strain rates. Based on the variations of  $\epsilon_c$  with temperatures and strain rates, the PLC effect may be determined as either “normal” or “inverse”. A discernible trend for the variations of  $\epsilon_c$  with temperatures and strain rates is observed in Fig. 2. After the onset of type A and A + B serrations,  $\epsilon_c$  decreases dramatically with increasing temperatures at the strain rates investigated. The value of  $\epsilon_c$  for the occurrence of type A and type A + B serrations becomes smaller at higher temperatures with a constant strain rate and decreases with lowering strain rates at the same temperature, indicating the characteristics of the normal PLC effect. It is also noted that the  $\epsilon_c$  for the onset of type B and C serrations shows very weak dependence on temperatures and strain rates.

**Table 1**

Summary of types of serrations observed on true stress-strain curves at various temperatures and strain rates.

$\dot{\epsilon}$ ( $\text{s}^{-1}$ )	Temperature (K)							
	300	573	623	673	773	873	923	973
$3 \times 10^{-3}$	N	N + A	A	A	A + B	B	B + C	C
$3 \times 10^{-4}$	N	A	A + B	A + B	B	B + C	C	C
$3 \times 10^{-5}$	–	A + B	B	B	B + C	C	–	–

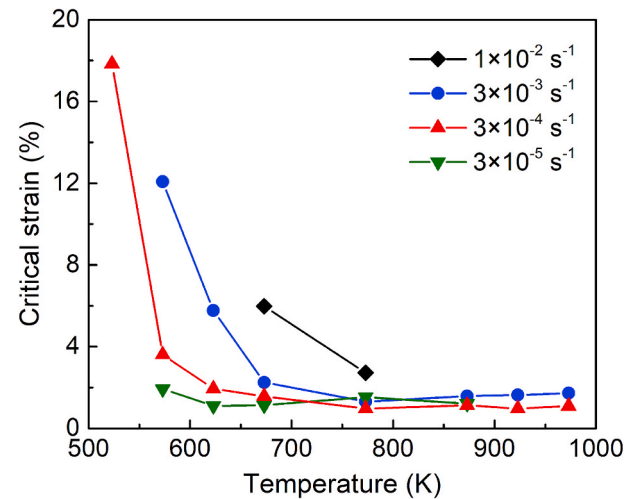


**Fig. 2.** Variation of the critical strain for serrated flow. Variation of critical plastic strain for the onset of serrations with temperature at different strain rates.

### 3.2. Activation energy

The solute elements considered to be interacting with dislocations in the DSA regime are usually assessed by comparing the activation energy for serrated flow with the activation energy for diffusion of solute elements in the matrix. The activation energy for the serrated flow is determined from the slopes of  $\ln\dot{\epsilon}_c$  vs.  $\ln(\epsilon_c)$  and  $\ln(\epsilon_c)$  vs.  $1/T$  plots as described by the following relationship [31]:

$$\epsilon_c^{m+\beta} = K\dot{\epsilon}\exp(Q/RT) \quad (1)$$

where  $Q$  is the activation energy for serrated flow,  $m$  and  $\beta$  are the exponents indicating the variations of vacancy concentration ( $C_v$ ) and mobile dislocation density ( $\rho_m$ ) with plastic strain (i.e.  $C_v \propto \epsilon^m$  and  $\rho_m \propto$

$\epsilon^\beta$ , respectively),  $K$  is a constant,  $R$  is the gas constant, and  $T$  is the absolute temperature. Within the normal PLC  $T$ - $\dot{\epsilon}$  regime, slopes of the plots of  $\ln \dot{\epsilon}$  vs.  $\ln(\epsilon_c)$  yield the values of the exponent ( $m + \beta$ ), which are typical of in the range of 2–3 (see Fig. 3a). With the average value of ( $m + \beta$ ) obtained from Fig. 3a, the activation energy for serrated flow was determined from the plot of  $\ln(\dot{\epsilon}_c)$  versus  $1/T$  where  $Q = \text{slope} \times (m + \beta) \times R$ , as shown in Fig. 3b. The average activation energy for serrated flow thus calculated using an average value ( $m + \beta$ ) of 2.63 is  $\sim 104$  kJ/mol. On the first appearance it is higher than the activation energies for the onset of the serrated flow for Waspalloy (55–66 kJ/mol) [22], Inconel 600 (55 kJ/mol) [21], and Inconel 718 (42 kJ/mol) [21]. Carbon is considered to be responsible for DSA effects in these Ni alloys as the activation energies inferred from the serrated flow in them is close to that for the pipe diffusion of C in Ni (69 kJ/mol). In addition, the  $m + \beta$  value is also an indicator for the responsible solutes for the serrated flow [3,4,6,11,13]. For DSA induced by substitutional solutes, values of  $m + \beta$  ranging from 2 to 3 have been reported, whereas for DSA due to interstitial atoms (i.e., C),  $m + \beta$  is usually closer to unity [3,4,13]. In the present 230 alloy, the calculated  $m + \beta$  values lie between 2 and 3 in the temperature range of 573–773 K, indicating a substitutional diffusion-controlled mechanism of DSA. Based on above results, it seems that substitutional atoms, such as Cr, Co and Mo, rather than interstitial atom C, might be responsible for the apparent PLC effect of the 230 alloy.

### 3.3. Microstructural characterization

#### 3.3.1. Bright-field TEM and atomic-resolution imaging

In order to verify the possible solute atoms involved in the normal PLC regime, TEM combined with high resolution EDX was utilized to explore the solute species which may be responsible for the serrated flow. Cui et al. [15] and Xu et al. [14] investigated a Ni–Co-based superalloy with a low stacking fault energy (SFE) and indicated that the normal behavior is associated with conventional DSA due to dynamic dislocation–solute interaction, while the inverse behavior may be related to the formation of stacking faults (SFs). Cai et al. [5] concluded that the micro-deformation mechanism switched from the formation of full dislocations to SFs with the increasing temperature or decreasing strain rate as the stress serration switches from type A to type C in Ni-based superalloys. Nevertheless, an earlier study by Han et al. [32] found that Suzuki segregation resulted in continuously serrated plastic flow for deformation at temperatures from 723 to 943 K with a strain rate of  $1.0 \times 10^{-4} \text{ s}^{-1}$  in a Co–Ni–Cr based superalloy. In the present work, TEM characterization was performed on the specimens deformed at temperatures of 773, 873 and 973 K with the strain rate of  $3 \times 10^{-3} \text{ s}^{-1}$ , and the corresponding bright-field TEM images of the typical microstructure are shown in Fig. 4a–c. Similar microstructural characteristics were observed. The microstructure of the samples deformed at

temperatures of 773–973 K is characterized by high densities of SFs, indicating that there is no transition on the deformation mechanism as the stress serrations switches from type A + B to C. The prevailing SFs highlight the fact that the present 230 alloy possesses a low SFE [33].

In detail, Fig. 5a shows an example of the bright-field TEM image of the defects in the sample tensile loaded at 773 K with a strain rate of  $3 \times 10^{-3} \text{ s}^{-1}$ . Profuse planar defects within grain interiors are aligned on two inclined planes with an acute angle of  $70.5^\circ$ , as indicated by the red and blue arrows. Close inspection by atomic-resolution TEM imaging along  $[110]$  zone axis reveals that the planar defects on such inclined planes are SFs on conjugate/various  $\{111\}$  planes (see Fig. 5b). The low SFE facilitated the dissociation of dislocations into the SFs bounded by Shockley partial dislocations, as revealed by a detailed analysis on the Burgers circuits surrounding each end of the SF in Fig. 5d according to Howe et al. [34]. In addition, the intersection and interaction of SFs on different  $\{111\}$  planes lead to the formation of V-like configurations, as indicated by the yellow arrows (S1) in Fig. 5b. Stacking sequence analysis reveals that the V-like SF intersection (S1) is formed by the interaction of two one-layer SFs (see Fig. 5c1). Detailed analyses on the Burgers circuits per the well-established methodology [35,36] displayed in Fig. 5c1 indicates that the V-like S1 stems from the interaction of two Shockley dislocations  $\frac{a}{6}[\bar{1}2\bar{1}]$  and  $\frac{a}{6}[211]$  enclosing the intersected SF 1 and 2 on inclined two  $\{111\}$  planes, respectively. As the two Shockley dislocations approach, the interaction of these two dislocations enables the formation of a sessile stair-rod dislocation by the following reaction:  $\frac{a}{6}[\bar{1}2\bar{1}] + \frac{a}{6}[211] \rightarrow \frac{a}{6}[\bar{1}\bar{1}0]$ , as depicted in Fig. 5c2. Therefore, the observed V-like configuration corresponds to a Lomer-Cottrell (L-C) lock with a sessile stair-rod dislocation. In summary, the observed high density of SFs suggests that the serrated flow of the present 230 alloy is induced by the pinning effect exerted on the SFs by solute atoms, i.e., Suzuki pinning effect [37–42].

#### 3.3.2. High-resolution EDX spectroscopy

EDX mapping was further conducted to detect chemical fluctuations of various elements across the SFs. Fig. 6a shows an example of high-resolution HAADF image and elemental maps collected from the area including two SFs (I: one-layer SF and II: two-layer SF). The high-resolution HAADF imaging and EDX mapping were operated at  $\langle 110 \rangle$  zone axis to ensure  $\{111\}$  atomic planes of the SFs edged on. The EDX mapping was performed over an area of  $7 \text{ nm} \times 7 \text{ nm}$  with an interval of 0.01023 nm for the data collection. On first appearance, both the one-layer and two-layer SFs exhibit enhanced intensities in the Cr and Co elemental maps, indicating enrichments of Cr and Co atoms at these two SFs. The compositional profiles obtained from the rectangular area with the dimension of  $5 \text{ nm} \times 3 \text{ nm}$  to across the two SFs are displayed in Fig. 6b, where each data point has been integrated along the SFs over the rectangular area to enhance the signal-to-noise ratio. It can be seen that quantitative analysis complies with the preliminary results

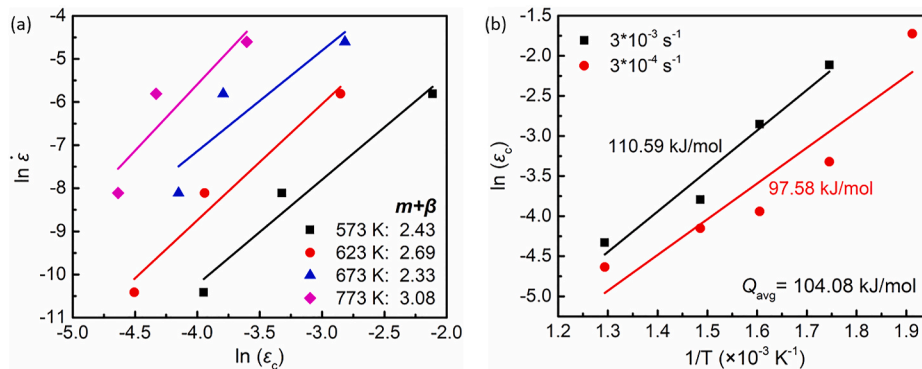
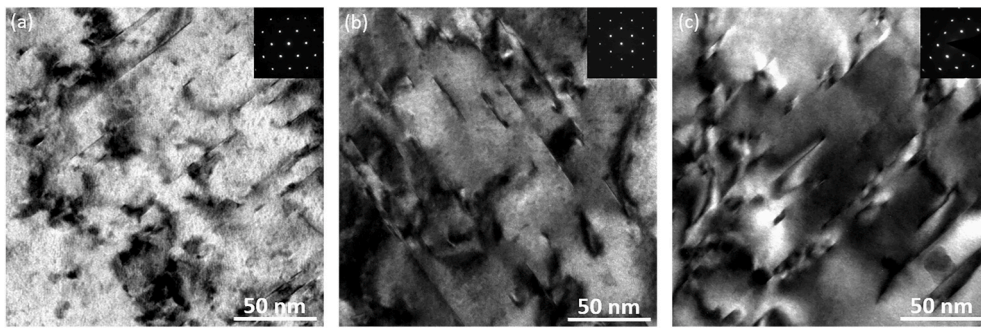
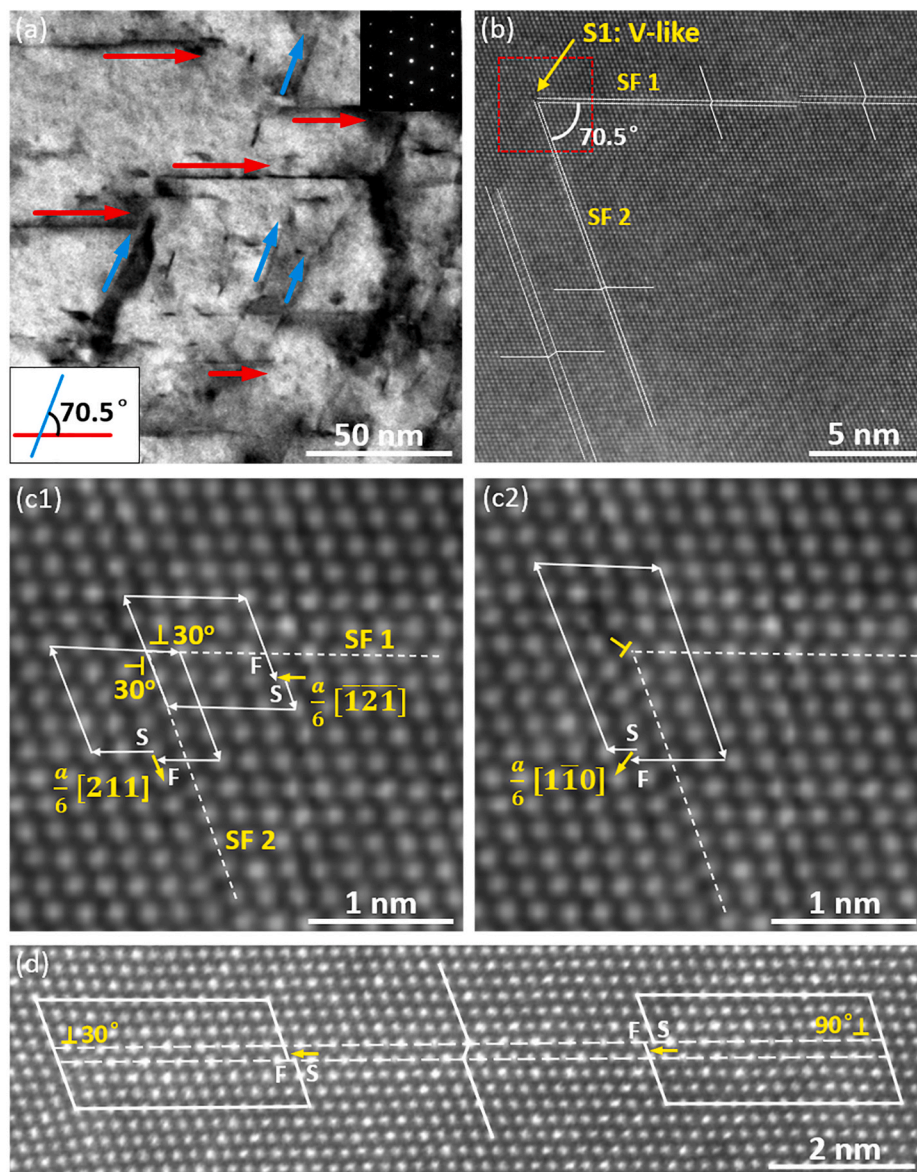


Fig. 3. Calculation of the activation energy for serrated flow. Calculated method of the activation energy: (a) Plot of  $\ln \dot{\epsilon}$  versus  $\ln(\epsilon_c)$  and (b) Plot of  $\ln(\epsilon_c)$  versus  $1/T$ .



**Fig. 4. Overall TEM investigation of the microstructures after tensile deformation.** The bright-field TEM images of the microstructure in the samples deformed with the strain rate of  $3 \times 10^{-3} \text{ s}^{-1}$  at: (a) 773 K, (b) 873 K and (c) 973 K corresponding to serration types of A + B, B and C.



**Fig. 5. Detailed TEM investigation of the microstructures after tensile deformation.** (a) The bright-field TEM image of the microstructure viewed along [110] zone axis, (b) the atomic-resolution TEM image and (c1), (c2) the detailed analyses on the Burgers circuits surrounding a sessile stair-rod dislocation and (d) a schematic showing a typical SF projected along the [110] direction in the sample deformed at 773 K with a strain rate of  $3 \times 10^{-3} \text{ s}^{-1}$ .

observed on the EDX mapping, i.e., Cr and Co atoms have segregated to the SFs by replacing Ni atoms. For W and Mo, no discernible segregation at the SFs was observed. This finding agrees with the phase-field

simulation of Suzuki segregation in a Co–Ni-based superalloy, suggesting the strong tendency of Cr and Co atoms segregating to the SF [43]. In summary, this segregation of solute atoms to SFs (i.e., Suzuki

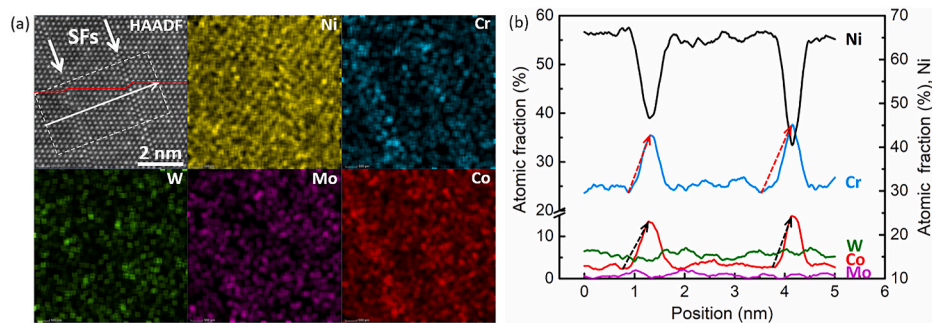


**Fig. 6. Atomic-resolution EDX investigation of the microstructures after tensile deformation.** (a) A high-resolution HAADF image of two edge-on SFs viewed along  $\langle 110 \rangle$  zone axis in a specimen deformed at 773 K and corresponding elemental EDX maps and (b) compositional profiles integrated along the SFs over the rectangular area with the dimension of 5 nm  $\times$  3 nm.

segregation) and the consequent interaction between solute atoms and SFs might contribute to the serrated flow as discussed below, inducing the periodic stress serrations. In addition, the direct evidence of solute atom segregation could be used for the validation of the dominant solute atoms responsible for Suzuki segregation deduced by the activation energy.

## 4. Discussion

### 4.1. Activation energy for serrated flow

Serrated flow characterized by type A and B serrations is always referred to as the normal PLC effect, while that with type C serrations is recognized as inverse PLC effect. Whereas the understanding of type-C unlocking serrations (inverse PLC) has not been very clear, most of the theoretical models based on DSA have been successful in explaining the normal PLC. For the onset of type A to B serrations at lower temperatures in alloy 230 displayed in Fig. 2,  $\varepsilon_c$  decreased rapidly with increasing temperatures at both strain rates investigated up to 773 K. The value of  $\varepsilon_c$  for the onset of type A/A + B/B serrations is greater at higher strain rates and decreases with increasing temperatures, indicating the occurrence of the normal PLC effect.  $\varepsilon_c$  then changed less severely with decreasing strain rates and increasing temperatures above 773 K, denoting the occurrence of type C serrations. The disappearance of serrations from the flow curve occurs in the high-temperature regime by either a progressively longer strain to the onset of serrations (a critical-strain-delay mechanism) or by a progressively smaller strain to the disappearance of serrations (disappearance off the end of the flow curve). In the present work, the latter condition was found when type C serrations gradually disappeared from the curve where the activation energy was improbable to be determined by  $\varepsilon_c$ . The calculation performed by Barnett et al. suggests that binding force between a dislocation and a solute atmosphere could decrease sharply with increasing temperatures [44]. Therefore, it is understandable that the disappearance of type-C serrations in alloy 230 occurs above a critical temperature when the binding force reduction dominates over the solute segregation [11]. In this case, we determined the average value of the activation energies for temperatures ranging from 523 to 773 K (normal PLC) in the 230 alloy to be 104 kJ/mol.

Generally, the solute atoms responsible for the DSA effect are identified by a comparison of the activation energy for serrated flow with that for solute atoms diffusion [3,4,6–8,11–13]. In alloy 625 (Cr, Mo, Fe, Nb as major alloying elements) [9] and UNS N10276 (Cr, Mo, Fe as major alloying elements) [12], the average activation energy for serrated flow at temperatures lower than 823 K and 873 K is calculated to be 98 and 132 kJ/mol in the normal DSA regime, respectively, indicating the diffusion of Mo atoms in both Ni alloys. The activation energy calculated by Han and co-workers in Nimonic 263 alloy (Co, Cr, Mo as major alloying elements) is 68 kJ/mol for the normal PLC effect, and

substitutional solutes such as Cr and Mo atoms were identified to be responsible for the PLC effect [4]. In alloy Inconel 617, the diffusion of the major substitutional elements Cr, Co and Mo were speculated to cause PLC effect based on the measured activation energy of 101 kJ/mol [7]. The consensus reached in these literatures is that activation energies for the onset of serrated flow are approximately 30%–60% of those for the lattice diffusion of Cr (289 kJ/mol), Co (284 kJ/mol) and Mo (213 kJ/mol) in Ni. The deduction for the solute species for the serrated flow is made based on an assumption that the segregation process is dominated by the pipe diffusion of solute atoms with lower activation energy than lattice diffusion [3,4,6,8,13]. In the present 230 alloy, the activation energy for the onset of serrated flow is calculated to be 104 kJ/mol, approximately 35%–50% of the activation energies for the lattice diffusion of Cr, Co and Mo atoms in Ni. Obviously, this measured activation energy suggests that Cr, Co and Mo atoms all might contribute to the segregation at SFs via pipe diffusion. This inference is further clarified by the observed segregation of Cr and Co at SFs. In summary, the measured activation energy and the TEM observations together lead us to conclude that the segregation of Cr and Co atoms at the SFs induce the serrated flow in the normal PLC regime.

### 4.2. Segregation mechanism

As has been widely accepted for DSA effect, the occurrence of the serrated flow stems from pinning and unpinning processes between mobile dislocations and solute atoms. Due to the segregation of solute atoms to the SFs in the present Ni alloy during tensile deformation at 773 K, the SF tends to attain an elemental composition different from the surrounding unfaulted area to lower the total energy of the SF [23]. When split dislocations glide to carry the plastic strain, the compositional difference could exert a pinning effect on the partially dissociated dislocations [23], leading to the stress rise associated with the upward serrations. Moreover, the flow drops of serrations occur when the dissociated dislocations successfully overcome the pinning strength of the solutes with assistance of the applied stress [45]. Nonetheless, based on the models proposed by Sleswyk [30] and Mulford [46], the segregation of the solute atoms to the dislocations took place during their waiting time ( $t_w$ ) at obstacles, which is manifested as the time lasting for one upward serration [11,19,31]. In the present case, the “ageing” of the SFs could take place during the waiting time for the SFs interaction with each other. An average  $t_w$  was determined to be 0.23 s based on the  $t_w$  for each serration over the entire flow curve at 773 K with a strain rate of  $3 \times 10^{-3} \text{ s}^{-1}$ . Such short time scale for the segregation of solute atoms to the SFs raises an important question concerning the diffusion process itself. The first possible scenario is that diffusion occurs perpendicular to the SFs. If so, along the diffusion direction, the chemical concentration of Cr varies from 25 to 37 at.%. The variation of the number of atoms along the diffusion direction is neglectful. The mean displacement of the Cr atoms, considered as the equivalent

diffusion distance during the diffusion process is calculated by  $\lambda = [\sum_{i=0}^N (C_i - C_1) d_i] / [\sum_{i=0}^N (C_i - C_1)]$  [47], where  $C_i$  is the Cr concentration at position  $i$ ,  $C_1$  is the Cr concentration in the non-segregation region of the matrix, and  $d_i$  is the horizontal axis of position  $i$ . ( $C_i - C_1$ ) is the concentration difference of Cr at position  $i$  and the matrix. This estimate gives a mean diffusion distance of the Cr atoms segregating from the non-segregation region of 0.57 nm to the SFs in Fig. 6b. Similarly, 0.61 nm diffusion distance is obtained for Co atoms. Thermo-calc 2020a software with TCNI9 and MOBNI5 databases [48] was utilized to determine the diffusion coefficients of Cr, Co, Mo and W in Ni matrix as  $1.10 \times 10^{-23}$ ,  $1.35 \times 10^{-23}$ ,  $1.04 \times 10^{-23}$  and  $1.12 \times 10^{-24}$  m<sup>2</sup> s<sup>-1</sup> at 773 K, respectively. Corresponding diffusion distances (estimated as  $(Dt_w)^{1/2}$ ) for this small-time scale of one upward serration are listed in Table 2. Note that these bulk diffusion coefficients only correspond to very short diffusion distances on the order of  $10^{-3}$  nm. For example, Cr atoms would only diffuse by a distance of 0.0016 nm, which is two orders of magnitude lower than the requested diffusion distance via diffusion perpendicular to the SFs. The second scenario is that diffusion of Co and Cr solute atoms occurs parallel or along the SFs. However, the discernible enrichment of Cr and Co atoms at the SFs on the EDX maps in Fig. 6a indicates that the enrichments of Cr and Co along the SFs should have at least prevailed through the thickness of TEM specimen, suggesting that diffusion distances should have been at least on the order of several nanometers. Therefore, these small diffusion distances resulting from the bulk diffusion can not enable the achievement of the local compositions exhibited by the SFs shown in Fig. 6. Actually, faster diffusion rates along the dislocation cores of partial dislocations, i.e., pipe diffusion, may also serve as a diffusion channel to facilitate the flow of solute species necessary for lowering the energy of the SFs.

## 5. Conclusions

Tensile behavior of a Ni alloy 230 has been studied at temperatures ranging from 300 K to 973 K with strain rates of  $1 \times 10^{-2}$ ,  $3 \times 10^{-3}$ ,  $3 \times 10^{-4}$  and  $3 \times 10^{-5}$  s<sup>-1</sup>, and the characteristics of serrated flow is present. Suzuki segregation has been observed in the sample tensile-deformed at 773 K by the HAADF imaging combined with high-resolution EDX mapping. The following conclusions can be drawn:

1. The measurement of the activation energy,  $Q$ , for the onset of serrated flow in the normal PLC regime is determined by the plots of the critical strain for serrated flow,  $\varepsilon_c$ , vs. strain rates and temperatures. The calculated value, 104 kJ/mol, for temperatures from 523 to 773 K is about 35%–50% of the activation energy for lattice diffusion of Cr, Co and Mo in Ni, implying that Cr, Co and Mo atoms might contribute to the segregation at SFs via pipe diffusion.
2. The segregation of substitutional Cr and Co atoms and the deficiency of Ni at SFs at 773 K with the strain rate of  $3 \times 10^{-3}$  s<sup>-1</sup> indicates that the DSA effect in alloy 230 at 773 K results from dynamic interactions between dissociated dislocations and solute atoms (Cr, Co).
3. The calculated diffusion distances within the ageing time of one upward serration at 773 K are not sufficient to achieve the observed segregation at SFs, indicating that the diffusion mechanism during the tensile process at 773 K may be the pipe diffusion along the partial dislocations.

## Data availability

The data that support the findings of this study are available from the corresponding author on reasonable request.

## CRedit authorship contribution statement

**Zhouwen Jiang:** Investigation, Formal analysis, Writing – original

**Table 2**

The diffusion distances (in nm) for main elements in the matrix for 0.23 s within the ageing time of a serration at 773 K.

Elements	Cr	W	Mo	Co
Distance (nm)	0.0016	0.00051	0.0015	0.0018

draft. **Lilong Zhu:** Formal analysis, Software. **Lianxu Yu:** Resources, Formal analysis. **Baoan Sun:** Methodology, Validation. **Yang Cao:** Investigation, Formal analysis. **Yonghao Zhao:** Supervision, Formal analysis. **Yong Zhang:** Conceptualization, Writing – review & editing.

## Declaration of competing interest

The authors declare that they have no known competing financial interests or personal relationships that could have appeared to influence the work reported in this paper.

## Acknowledgements

This work was supported by the Ministry of Science and Technology of China (grant numbers 2017YFA0204403), the National Natural Science Foundation of China (grant number 51601091, 51971112 and 52071181), the Natural Science Foundation of Jiangsu Province (grant number BK 20160826), the Six Talent Peaks Project of Jiangsu Province (grant number 2017-XCL-051), the Fundamental Research Funds for the Central Universities (grant numbers 30917011106 and 30919011405), and Jiangsu Provincial Key Research and Development Program (BE2020085). Lilong Zhu acknowledges the financial support from the Taishan Scholars Program of Shandong Province (No. Tsqn201909081) and State Key Laboratory of Powder Metallurgy (Central South University, Changsha, China).

## References

- [1] K. Hrutkay, D. Kaoumi, Tensile deformation behavior of a nickel based superalloy at different temperatures, *Mater. Sci. Eng., A* 599 (2014) 196–203, <https://doi.org/10.1016/j.msea.2014.01.056>.
- [2] P. Rodriguez, Serrated plastic flow, *Bull. Mater. Sci.* 6 (1984) 653–663, <https://doi.org/10.1007/BF02743993>.
- [3] V. Shankar, M. Valsan, K.B.S. Rao, S.L. Mannan, Effects of temperature and strain rate on tensile properties and activation energy for dynamic strain aging in Alloy 625, *Metall. Mater. Trans. A* 35 (2004) 3129–3139, <https://doi.org/10.1007/s11661-004-0057-0>.
- [4] G. Han, C. Tian, C. Cui, Z. Hu, X. Sun, Portevin–Le chatelier effect in nimonic 263 superalloy, *Acta Metall. Sin.* 28 (5) (2015) 542–549, <https://doi.org/10.1007/s40195-015-0230-z>.
- [5] Y. Cai, C. Tian, G. Zhang, G. Han, S. Yang, S. Fu, C. Cui, Q. Zhang, Influence of  $\gamma'$  precipitates on the critical strain and localized deformation of serrated flow in Ni-based superalloys, *J. Alloys Compd.* 690 (2017) 707–715, <https://doi.org/10.1016/j.jallcom.2016.08.194>.
- [6] E. Pu, W. Zheng, Z. Song, H. Feng, F. Yang, H. Dong, Effects of temperature and strain rate on tensile deformation behavior of superalloy UNS N10276, *Mater. Sci. Eng., A* 699 (2017) 88–98, <https://doi.org/10.1016/j.msea.2017.05.085>.
- [7] C.V. Rao, N.C.S. Srinivas, G.V.S. Sastry, V. Singh, Dynamic strain aging, deformation and fracture behaviour of the nickel base superalloy Inconel 617, *Mater. Sci. Eng., A* 742 (2019) 44–60, <https://doi.org/10.1016/j.msea.2018.10.123>.
- [8] Y. Cao, C. Zhang, C. Zhang, H. Di, G. Huang, Q. Liu, Influence of dynamic strain aging on the mechanical properties and microstructural evolution for Alloy 800H during hot deformation, *Mater. Sci. Eng., A* 724 (2018) 37–44, <https://doi.org/10.1016/j.msea.2018.03.074>.
- [9] H. Jiang, Q. Zhang, X. Chen, Z. Chen, Z. Jiang, X. Wu, J. Fan, Three types of portevin–Le chatelier effects: experiment and modelling, *Acta Mater.* 55 (7) (2007) 2219–2228, <https://doi.org/10.1016/j.actamat.2006.10.029>.
- [10] R. Zhang, C. Tian, C. Cui, Y. Zhou, X. Sun, Portevin–Le Chatelier effect in a wrought Ni–Co based superalloy, *J. Alloys Compd.* 818 (2020) 152863, <https://doi.org/10.1016/j.jallcom.2019.152863>.
- [11] K. Gopinath, A.K. Gogia, S.V. Kamat, U. Ramamurty, Dynamic strain ageing in Ni-base superalloy 720Li, *Acta Mater.* 57 (4) (2009) 1243–1253, <https://doi.org/10.1016/j.actamat.2008.11.005>.
- [12] S.A. Nalawade, M. Sundararaman, R. Kishore, J.G. Shah, The influence of aging on the serrated yielding phenomena in a nickel-base superalloy, *Scripta Mater.* 59 (9) (2008) 991–994, <https://doi.org/10.1016/j.scriptamat.2008.07.004>.

- [13] C.L. Hale, W.S. Rollings, M.L. Weaver, Activation energy calculations for discontinuous yielding in Inconel 718SPF, *Mater. Sci. Eng., A* 300 (2001) 153–164, [https://doi.org/10.1016/S0921-5093\(00\)01470-2](https://doi.org/10.1016/S0921-5093(00)01470-2).
- [14] Y.J. Xu, D.Q. Qi, K. Du, C.Y. Cui, H.Q. Ye, Stacking fault effects on dynamic strain aging in a Ni-Co-based superalloy, *Scripta Mater.* 87 (2014) 37–40, <https://doi.org/10.1016/j.scriptamat.2014.05.012>.
- [15] C.Y. Cui, Y.F. Gu, Y. Yuan, H. Harada, Dynamic strain aging in a new Ni-Co base superalloy, *Scripta Mater.* 64 (6) (2011) 502–505, <https://doi.org/10.1016/j.scriptamat.2010.11.025>.
- [16] W. Chen, M.C. Chaturvedi, On the mechanism of serrated deformation in aged Inconel 718, *Mater. Sci. Eng., A* 229 (1997) 163–168, [https://doi.org/10.1016/S0921-5093\(97\)00005-1](https://doi.org/10.1016/S0921-5093(97)00005-1).
- [17] K. Gopinath, A.K. Gogia, S.V. Kamat, R. Balamuralikrishnan, U. Ramamurty, Tensile properties of Ni-Based superalloy 720Li: temperature and strain rate effects, *Matall. Mater. Trans. A* 39 (10) (2008) 2340–2350, <https://doi.org/10.1007/s11661-008-9585-3>.
- [18] Y. Liu, Y. Cai, C. Tian, G. Zhang, G. Han, S. Fu, C. Cui, Q. Zhang, Experimental investigation of a Portevin-Le Chatelier band in Ni-Co-based superalloys in relation to  $\gamma'$  precipitates at 500 °C, *J. Mater. Sci. Technol.* 49 (2020) 35–41, <https://doi.org/10.1016/j.jmst.2020.02.001>.
- [19] Y. Zhang, J.P. Liu, S.Y. Chen, X. Xie, P.K. Liaw, K.A. Dahmen, J.W. Qiao, Y. L. Wang, Serration and noise behaviors in materials, *Prog. Mater. Sci.* 90 (2017) 358–460, <https://doi.org/10.1016/j.pmatsci.2017.06.004>.
- [20] P. Zhang, Y. Yuan, Z.H. Gao, Y.F. Gu, J. Li, J.B. Yan, X.F. Gong, J.T. Lu, X.B. Shi, B. Q. Fu, Strain-rate insensitive yield strength and deformation mechanisms of Ni-base superalloy CM247LC at 600 °C, *J. Alloys Compd.* 862 (2021) 158478, <https://doi.org/10.1016/j.jallcom.2020.158478>.
- [21] R.W. Hayes, On a proposed theory for the disappearance of serrated flow in F.C.C. Ni alloys, *Acta Metall.* 31 (1983) 365–371, [https://doi.org/10.1016/0001-6160\(83\)90213-4](https://doi.org/10.1016/0001-6160(83)90213-4).
- [22] R.W. Hayes, W.C. Hayes, On the mechanism of delayed discontinuous plastic flow in an age-hardened Nickel alloy, *Acta Metall.* 30 (1982) 1295–1301, [https://doi.org/10.1016/0001-6160\(82\)90148-1](https://doi.org/10.1016/0001-6160(82)90148-1).
- [23] J. Weertman, J.R. Weertman, *Elementary Dislocation Theory*, Oxford University, New York, Oxford, 1992.
- [24] S. Fu, T. Cheng, Q. Zhang, Q. Hu, P. Cao, Two mechanisms for the normal and inverse behaviors of the critical strain for the Portevin–Le Chatelier effect, *Acta Mater.* 60 (19) (2012) 6650–6656, <https://doi.org/10.1016/j.actamat.2012.08.035>.
- [25] Q. Hu, Q. Zhang, P. Cao, S. Fu, Thermal analyses and simulations of the type A and type B Portevin–Le Chatelier effects in an Al–Mg alloy, *Acta Mater.* 60 (4) (2012) 1647–1657, <https://doi.org/10.1016/j.actamat.2011.12.003>.
- [26] S.H. Fu, Y.L. Cai, S.L. Yang, Q.C. Zhang, X.P. Wu, The mechanism of critical strain of serrated yielding in strain rate domain, *Chin. Phys. Lett.* 33 (2016), 026201, <https://doi.org/10.1088/0256-307X/33/2/026201>.
- [27] W.F. Gale, T.C. Totemeier, *Smithells Metals Reference Book*, Butterworth-Heinemann, London, 2004.
- [28] B.J. Brindley, J.T. Barnby, Dynamic strain ageing in mild steel, *Acta Metall.* 14 (1966) 1765–1780, [https://doi.org/10.1016/0001-6160\(66\)90028-9](https://doi.org/10.1016/0001-6160(66)90028-9).
- [29] B.J. Brindley, The effect of dynamic strain-ageing on the ductile fracture process in mild steel, *Acta Metall.* 18 (1970) 325–329, [https://doi.org/10.1016/0001-6160\(70\)90147-1](https://doi.org/10.1016/0001-6160(70)90147-1).
- [30] A.W. Sleseswyk, Slow strain-hardening of ingot iron, *Acta Metall* 6 (1958) 598–603, [https://doi.org/10.1016/0001-6160\(58\)90101-9](https://doi.org/10.1016/0001-6160(58)90101-9).
- [31] P.G. McCormick, A model for the Portevin–Le Chatelier effect in substitutional alloys, *Acta Metall.* 20 (1972) 351–354, [https://doi.org/10.1016/0001-6160\(72\)90028-4](https://doi.org/10.1016/0001-6160(72)90028-4).
- [32] G.W. Han, I.P. Jones, R.E. Smallman, Direct evidence for Suzuki segregation and Cottrell pinning in MP159 superalloy obtained by FEG(S)TEM/EDX, *Acta Mater.* 51 (10) (2003) 2731–2742, [https://doi.org/10.1016/S1359-6454\(02\)00359-2](https://doi.org/10.1016/S1359-6454(02)00359-2).
- [33] S.L. Shang, C.L. Zacherl, H.Z. Fang, Y. Wang, Y. Du, Z.K. Liu, Effects of alloying element and temperature on the stacking fault energies of dilute Ni-base superalloys, *J. Phys. Condens. Matter* 24 (50) (2012) 505403, <https://doi.org/10.1088/0953-8984/24/50/505403>.
- [34] J.M. Howe, U. Dahmen, R. Gronsky, Atomic mechanisms of precipitate plate growth, *Philos. Mag.* A 56 (1) (1987) 31–61, <https://doi.org/10.1080/01418618708204465>.
- [35] J.P. Hirth, J. Lothe, *Theory of Dislocations*, second ed., John Wiley & Sons, New York, USA, 1982.
- [36] D.L. Medlin, G.H. Campbell, C.B. Carter, Stacking defects in the 9R phase at an incoherent twin boundary in copper, *Acta Metall.* 46 (1998) 5135–5142, [https://doi.org/10.1016/S1359-6454\(98\)00164-5](https://doi.org/10.1016/S1359-6454(98)00164-5).
- [37] H. Suzuki, Segregation of solute atoms to stacking faults, *J. Phys. Soc. Jpn.* 17 (1962) 322–325, <https://doi.org/10.1143/jpsj.17.322>.
- [38] A. Chiba, X.G. Li, M.S. Kim, High work-hardening rate and deformation twinning of Co-Ni-based superalloy at elevated temperatures, *Philos. Mag.* A 79 (7) (1999) 1533–1554, <https://doi.org/10.1080/01418619908210378>.
- [39] A. Chiba, M.S. Kim, Suzuki segregation and dislocation locking in supersaturated Co-Ni-based alloy, *Mater. Trans.* 42 (2001) 2112–2116, <https://doi.org/10.2320/matertrans.42.2112>.
- [40] H. Bian, X. Xu, Y. Li, Y. Koizumi, Z. Wang, M. Chen, K. Yamanaka, A. Chiba, Regulating the coarsening of the  $\gamma'$  phase in superalloys, *NPG Asia Mater.* 7 (8) (2015) e212, <https://doi.org/10.1038/am.2015.96>, e212.
- [41] H. Bian, Y. Li, D. Wei, Y. Cui, F. Wang, S. Sun, K. Yamanaka, Y. Koizumi, A. Chiba, Precipitation behavior of a novel cobalt-based superalloy subjected to prior plastic deformations, *Mater. Des.* 112 (2016) 1–10, <https://doi.org/10.1016/j.matdes.2016.09.004>.
- [42] H. Bian, Y. Cui, Y. Li, A. Chiba, Y. Nie, The influence of Mo on Suzuki-segregation-related microstructure evolution and mechanical properties of Co–Ni-based superalloy, *J. Alloys Compd.* 768 (2018) 136–142, <https://doi.org/10.1016/j.jallcom.2018.07.154>.
- [43] Y. Koizumi, T. Nukaya, S. Suzuki, S. Kurosu, Y. Li, H. Matsumoto, K. Sato, Y. Tanaka, A. Chiba, Suzuki segregation in Co–Ni-based superalloy at 973K: an experimental and computational study by phase-field simulation, *Acta Mater.* 60 (6–7) (2012) 2901–2915, <https://doi.org/10.1016/j.actamat.2012.01.054>.
- [44] D.M. Barnett, G. Wong, W.D. Nix, The binding force between a peierls-nxbarro edge dislocation and a fermi-dirac solute atmosphere, *Acta Metall.* 30 (1982) 2035–2041, [https://doi.org/10.1016/0001-6160\(82\)90106-7](https://doi.org/10.1016/0001-6160(82)90106-7).
- [45] J. Friedel, *Dislocations*, Pergamon Press, London, 1964.
- [46] R.A. Mulford, U.F. Kocks, New observation on the mechanisms of dynamic strain aging and of jerky flow, *Acta Metall.* 27 (1979) 1125–1134, [https://doi.org/10.1016/0001-6160\(79\)90130-5](https://doi.org/10.1016/0001-6160(79)90130-5).
- [47] W. Guo, E.A. Jagle, P.P. Choi, J. Yao, A. Kostka, J.M. Schneider, D. Raabe, Shear-induced mixing governs codeformation of crystalline-amorphous nanolaminates, *Phys. Rev. Lett.* 113 (3) (2014), 035501, <https://doi.org/10.1103/PhysRevLett.113.035501>.
- [48] J.O. Andersson, T. Helander, L. Höglund, P. Shi, B. Sundman, Thermo-Calc & DICTRA, Computational tools for materials science, *Calphad* 26 (2002) 273–312, [https://doi.org/10.1016/S0364-5916\(02\)00037-8](https://doi.org/10.1016/S0364-5916(02)00037-8).